J Mater Sci: Mater Med (2010) 21:1445–1451
DOI 10.1007/s10856-010-4023-7

Zirconia-MWCNT nanocomposites for biomedical applications obtained by colloidal processing

N. Garmendia · I. Santacruz · R. Moreno · I. Obieta

Received: 29 October 2009 / Accepted: 1 February 2010 / Published online: 17 February 2010

Abstract Zirconia ceramics are widely used as femoral heads, but case studies show that delayed failure can occur in vivo due to crack propagation. The addition of carbon nanotubes (CNT) is aimed to avoid the slow crack propagation and to enhance the toughness of the ceramic material used for prostheses. However, to really enhance the mechanical properties of the material it is necessary to achieve a uniform distribution of the CNT in the zirconia matrix. Colloidal processing has demonstrated to be suitable for obtaining ceramic-based composites with homogeneous distribution of the phases and high green density. This work compares the colloidal behavior of the as-received multi wall carbon nanotubes (ar-MWCNT) and the partially coated MWCNT (pc-MWCNT) when immersed in a nanozirconia matrix. With pc-MWCNT an improvement in the dispersion is proved. Moreover, the sintered samples that contain pc-MWCNT show higher density, lower grain size, improved toughness and enhanced hardness under the same sintering cycle when compared to the samples with ar-MWCNT.

N. Garmendia (✉) · I. Obieta
Unidad de Salud, INASMET-TECNALIA, Paseo Mikeletegui 2, Parque Tecnológico, 20009 San Sebastián, Gipuzkoa, Spain
e-mail: ngarmend@inasmet.es

N. Garmendia · I. Obieta
Ciber-BBN, San Sebastián, Gipuzkoa, Spain

I. Santacruz · R. Moreno
Instituto de Cerámica y Vidrio, CSIC, C/Kelsen 5, 28049 Madrid, Spain

I. Santacruz
Departamento de Química Inorgánica, Cristalografía y Mineralogía, Universidad de Málaga, 29071 Málaga, Spain

1 Introduction

The yttria stabilized zirconia (YTZP) is a very attractive material for orthopaedic applications thanks to its excellent biocompatibility, high fracture toughness, high strength and low wear rates [1]. But case studies show that delayed failure can occur in vivo due to crack propagation [2, 3]. In order to improve the lifetime and the reliability of the prostheses carbon nanotubes (CNT) are added [4]. An increase in toughness is aimed with the incorporation of the CNT. Besides, a nanostructured YTZP matrix will be used. Nanocrystalline materials are expected to show improved mechanical properties [5] and the nanometric features in the surface of the prostheses seem to reduce the risk of rejection and to enhance the proliferation of osteoblasts (bone-forming cells) [6].

CNT have been of great interest since they were first described by Iijima in 1991 [7]. They appear to be promising reinforcing agents for ceramic matrix composites due to their high aspect ratios and their unique mechanical properties. Many authors report the manufacture of CNT-ceramic nanocomposites with enhanced hardness and toughness [8–14], while others do not achieve any real improvement [15, 16]. This is thought to be due to the existence of CNT agglomerates and clusters, which act as flaws in the matrix, and to the absence of a strong interfacial bonding between the CNT and the ceramic particles. These main drawbacks can be addressed by using zirconia coated multiwall carbon nanotubes (pc-MWCNT) and by handling the interparticle potentials through colloidal processing.

Although it is a widely used technique in the ceramic field, dry compaction of nanopowders is often difficult. Strong tendency to agglomerate, poor dispersion of second phases and small flowability have to be overcome. In addition, the colloidal processing approach allows the

preparation of CNT-ceramic concentrated suspensions for producing nanocomposites with a high dispersion level of the CNT into the ceramic matrix. However, the nature and strength of the interparticle forces and also the quantity, shape and size of the CNT to be dispersed determine the rheological properties of the suspensions.

In a previous work the development of YTZP with and without as received multiwall carbon nanotubes (ar-MWCNT) was studied by a colloidal process based on the heterocoagulation mechanism [17]. In this process, a strong electrostatic interaction between the two phases is promoted. A polyelectrolyte of opposite charge is adsorbed on each phase, so the difference in their isoelectric points is increased. This way, strong electrostatic forces appear and, as a result, the nanopowders attach to the CNT surfaces [18, 19]. The slip casting of these suspensions and the later sintering of the green bodies gave homogeneous YTZP and YTZP/ar-MWCNT samples [17]. A small enhancement on the Vickers' toughness was observed, which suggested the good behavior of CNT as strengthening agents for zirconia based materials. Anyhow, the need of functionalized CNT with a bonding between the CNT and the zirconia was highlighted.

In the present work, the colloidal processing of the pc-MWCNT is studied. The pc-MWCNT were obtained by the hydrothermal synthesis of zirconia nanoparticles in the presence of ar-MWCNT [20, 21], so a chemical bonding between ar-MWCNT and nanozirconia particles occurs [22, 23]. The colloidal behavior of both pc-MWCNT and ar-MWCNT in an aqueous medium are studied. The rheological properties of concentrated suspensions of YTZP, YTZP/ar-MWCNT and YTZP/pc-MWCNT are compared with special focus on the effect of pc-MWCNT on the forming performance and on the final properties of the material.

2 Experimental procedure

As ceramic material, a commercial 3 mol% yttria tetragonal zirconia polycrystalline nanopowder (YTZP) was used (Inframat Advanced Materials, USA), with a primary particle size of 30–60 nm and a specific surface area of 41.7 m^2/g. Ar-MWCNT (Sunnano, China) synthesized by CVD (Chemical Vapor Deposition) with an average diameter between 10 and 30 nm and length of up to 10 μm were used. They have a purity over 80%, with a low metal content (0.85% Fe, 0.82% Ni and 1.07% Al).

Pc-MWCNT were obtained by coating them with nanosized zirconia under hydrothermal conditions as described elsewhere [20–22]. Atomic Force Microscopy (AFM) imaging of the ar-MWCNT and pc-MWCNT were performed in a Digital Instruments Multimode AFM (Veeco, Santa Barbara, CA) with a Nanoscope III controller using tapping mode. The zeta potential values of ar-MWCNT, pc-MWCNT and YTZP were measured by laser Doppler velocimetry using a Zetasizer NanoZS (Malvern, UK) apparatus. Results were taken with caution only for comparison purposes. For the measurements, suspensions were prepared to a concentration of 0.001 wt% using 10^{-2} M KCl solutions as electrolyte, with and without deflocculants.

Diluted suspensions were prepared by adding either the ar-MWCNT or the pc-MWCNT to deionized water containing poly(ethylenimine), PEI, (Aldrich Chemical Company, USA). PEI provides a positive charge to the ar-MWCNT and the pc-MWCNT at the working pH (pH 8.0 ± 0.1). The suspensions were sonicated for two minutes [17]. In the case of the ar-MWCNT a concentration of 20 wt% PEI relative to ar-MWCNT was added according to previous studies [17]. In the case of pc-MWCNT, the addition of PEI was previously optimized through zeta potential measurements (0, 1.0, 2.0 and 4.0 wt% of PEI, which corresponds to 0, 10, 20 and 40 wt% relative to the ar-MWCNT).

After dispersing the ar-MWCNT or the pc-MWCNT, an ammonium salt of polyelectrolyte (PAA, Duramax D3005, Rohm & Haas, USA) was added to a concentration of 2 wt% on a dry mass basis prior to the incorporation of YTZP up to a solids loading of 65 wt%. The new suspension was ultrasonicated for eight minutes. Ar-MWCNT or pc-MWCNT were added to achieve a final concentration of 0.3 wt% (1 vol.%) relative to YTZP powder. The rheological behavior of the fresh and 24 h aged suspensions was studied using a rheometer (Model RS50, Thermo Haake, Karlsruhe, Germany) with a double-cone and plate system (60 mm in diameter, 2° cone angle), provided with a solvent trap to reduce evaporation. A three-stage measuring program was used, with a linear increase of shear rate from 0 to 1000 s^{-1} in 300 s, a plateau at 1000 s^{-1} for 120 s and a further decrease to zero shear rate in 300 s.

Slip-cast samples with 9 mm in diameter and 10 mm in thickness were obtained and left to dry for 24 h at room conditions. The green densities of the obtained green bodies (YTZP/ar-MWCNT and YTZP/pc-MWCNT) were measured with the Archimedes' method in mercury. The theoretical density (TD) of zirconia was considered as 6.10 g cm^{-3} (ASTM 83-113). Green fracture surfaces were observed by field emission scanning electron microscopy, FEG-SEM (LEO 1530VP, LEO Elektronenmikroskopie GmbH, Oberkochen, Germany).

Dynamic sintering tests of YTZP/ar-MWCNT and YTZP/pc-MWCNT specimens were performed in Argon atmosphere up to 1500°C with a heating rate of 5°C/min using a differential dilatometer (Setaram, Setsys TMA-18, Caluire, France). The specimens were sintered at 1350°C/1 h in Ar,

with a heating and a cooling rate of 250°C/h. The final densities were measured using the Archimedes' method in water. The sintered fracture surfaces were observed and the grain size was evaluated from scanning electron microscopy images (SEM JEOL JSM-5910-LV).

Hardness and fracture toughness of the samples were measured using Vickers' indentation tests. Three indentations were performed in each sample and three samples of each composition were tested. The indentation tests were performed applying a 5 kg load according to the UNE-EN ISO 6507-1:2006 standard. The indentation fracture toughness has become a very controversial method, especially in CNT-ceramic composites [24–26]. Nevertheless it is still a very common method used for zirconia ceramics and zirconia matrix composites [15, 16, 27]. Although it might not give the real toughness intensity factor it is very useful for comparing the toughness values of the materials [26, 28]. Moreover, it is a very effective method for obtaining the fracture threshold (K_{I0}) below which no crack propagation occurs. The K_{I0} value will give the safety range of use of the material in many applications, such as joint prostheses [29, 30]. So, the fracture threshold (K_{I0}) was calculated by measuring the crack length some days after the indentation, once the crack had reached the Griffith equilibrium [31]. For determining the fracture toughness the following expression by Anstis was used [32]:

$$K_{I0} = \chi \cdot P \cdot c_0^{-3/2} \quad (1)$$

$$\chi = C \cdot \left(\frac{E}{H}\right)^{1/2} \quad (2)$$

P is the applied force in Newtons and c_0 is the crack length. χ is a constraint factor defined by Anstis et al. [32], where C is a geometric constant that values 0.016, H is the Vickers hardness in GPa and E is the Young's modulus in GPa. The Young's modulus was assumed to be $E = 220$ GPa for all the samples, irrespective of their composition.

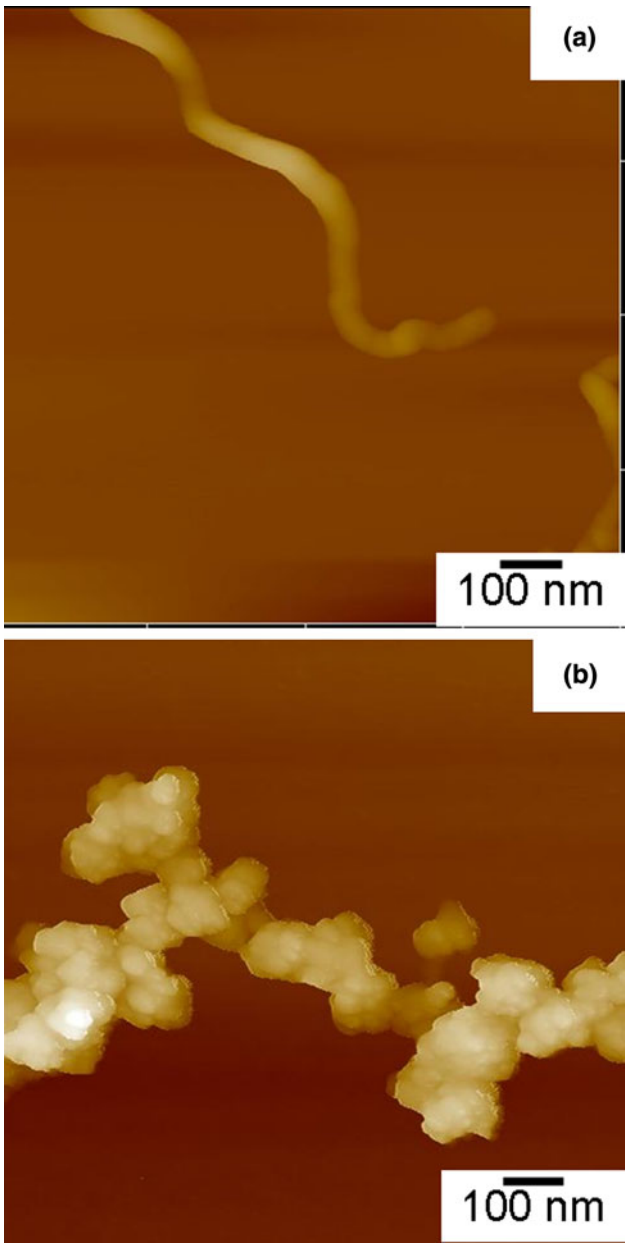

Fig. 1 AFM images of the (**a**) ar-MWCNT and (**b**) pc-MWCNT

3 Results and discussion

Figure 1 shows AFM images of both ar-MWCNT and pc-MWCNT. The zirconia coating, which is well adhered to the pc-MWCNT [21] surface, maintains the size (~50 nm) of the commercial zirconia powder so that no agglomeration occurs during the coating process.

Table 1 shows the zeta potential values of the pc-MWCNT suspensions obtained by the addition of different amounts of PEI, from 0 to 4 wt% (relative to pc-MWCNT). Suspensions with 1 or 2 wt% PEI show the highest absolute zeta potential values, which are positive, meaning those particles have a positive surface charge under those conditions. The surface behavior was studied as a function of pH and deflocculant content for aqueous suspensions of YTZP, ar-MWCNT and pc-MWCNT. Figure 2 shows the evolution of zeta potential with pH for the three materials without deflocculants. It can be seen that the isoelectric point (IEP) of the YTZP occurs at pH ~6, in good agreement with other values reported in the literature for nanosized YTZP powders [33]. The ar-MWCNT show an apparent IEP of ~7.5. However, for the pc-MWCNT the surface becomes similar to that of YTZP, therefore the IEP of pc-MWCNT is rather the same to that of YTZP. This suggests that stable suspensions could be prepared at either acidic or basic pH range

Table 1 Zeta potential values of pc-MWCNT with different PEI amounts

PEI (wt%)	Zeta potential (mV)	pH ± 0.1
0	9 ± 5	6.0
1	25 ± 6	8.2
2	31 ± 4	8.3
4	15 ± 5	8.8

(≤4 or ≥8). To ensure a good adhesion between YTZP and ar-MWNCT or pc-MWNCT, a strong electrostatic interaction is necessary. For this purpose, the YTZP were dispersed with 2 wt% PAA, an anionic polyelectrolyte. On the other hand, the ar-MWCNT were dispersed with 20 wt% PEI and pc-MWCNT were dispersed with 1 or 2 wt% PEI, a cationic polyelectrolyte. This way, opposite charges that favor the attraction are promoted. Figure 3 shows the variation of zeta potential with pH for suspensions of YTZP dispersed with PAA and the ar-MWCNT and pc-MWCNT dispersed with PEI. The addition of PAA to the YTZP shifted down its IEP about 3 pH units (until pH < 3), and in the case of both ar-MWCNT and pc-MWCNT, the addition of PEI shifted up about 3 units of pH (until pH > 9). In the case of pc-MWCNT suspensions the content of PEI was increased from 1 to 2 wt%. The addition of 2 wt% promoted a better stabilization to the pc-MWCNT at any pH value compared to 1 wt%, which is also accompanied with higher IEP values (∼10.5 and ∼9.5 for 2 and 1 wt% PEI, respectively), which means a larger range of pH where the CNT are positively charged.

After the adsorption of the differently charged polyelectrolytes on the YTZP and ar-MWCNT and pc-MWCNT, it can be observed that the former became negatively charged from pH > 3 and the ar-MWCNT and pc-MWCNT became positively charged up to pH ∼10.5. Thus there are more than 7 units of pH for the heterocoagulation process, in which strong electrostatic interaction occurs and more homogeneous coating is obtained. This

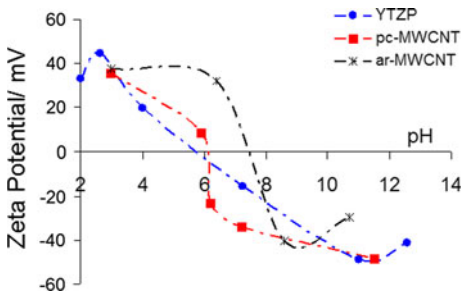

Fig. 2 Zeta potential curves as a function of pH of YTZP, ar-MWCNT and pc-MWCNT without deflocculants

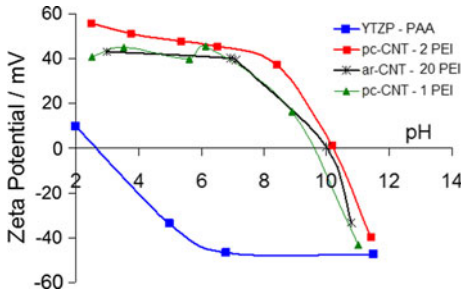

Fig. 3 Zeta potential curves as a function of pH of YTZP, ar-MWCNT and pc-MWCNT with deflocculants

will be especially significant if pH is controlled between pH 8 and pH 10, where the zeta potential changes from −40 to +40 mV.

Once the stability conditions were established, concentrated suspensions (65 wt% solids) of YTZP and mixtures of YTZP with 1 vol.% of either ar-MWCNT or pc-MWCNT were prepared. The flow curves of the as-prepared suspensions are plotted in Fig. 4a. As observed, the incorporation of a small amount of ar-MWCNT or pc-MWNCT has a strong effect on viscosity and thixotropy, although values maintain low enough to allow easy handling during preparation and slip casting. However, these suspensions have a significant ageing. Figure 4.b shows the flow curves of the same suspensions plotted in Fig. 4.a but measured after 24 h ageing. Suspensions were maintained under rotation in closed flasks to prevent drying and oxidation. The aged YTZP suspensions show a small thixotropy, demonstrating that some structure has been formed, which is usually observed with nanopowders. But, on the other hand, the suspensions containing the ar-MWCNT or pc-MWCNT have suffered a dramatic increase of viscosity and, in particular, a very broad hysteresis cycle appears. This cycle is even larger when ar-MWCNT are added, demonstrating that strong structure is formed in spite of the small addition of ar-MWCNT.

Figure 5 shows the green fracture surfaces of the slip cast YTZP/ar-MWCNT and YTZP/pc-MWCNT samples. In both cases, the CNT are homogeneously distributed and no bundles or agglomerates are observed. In addition, for the YTZP/pc-MWCNT samples the pc-MWCNT are completely immersed in the ceramic matrix, and they can be distinguished by the alignment of the YTZP particles attached by heterocoagulation. Anyhow, for the ar-MWCNT, this does not occur. The obtained green density is the same for both materials, as it is presented in Table 2. Figure 6 shows the results of the dynamic sintering study performed for both samples in an Argon atmosphere. Important differences are observed between them. The YTZP/pc-MWCNT show a higher shrinkage, and the maximum shrinkage (i.e. densification rate) occurs at a slightly lower temperature. This is in good agreement with their

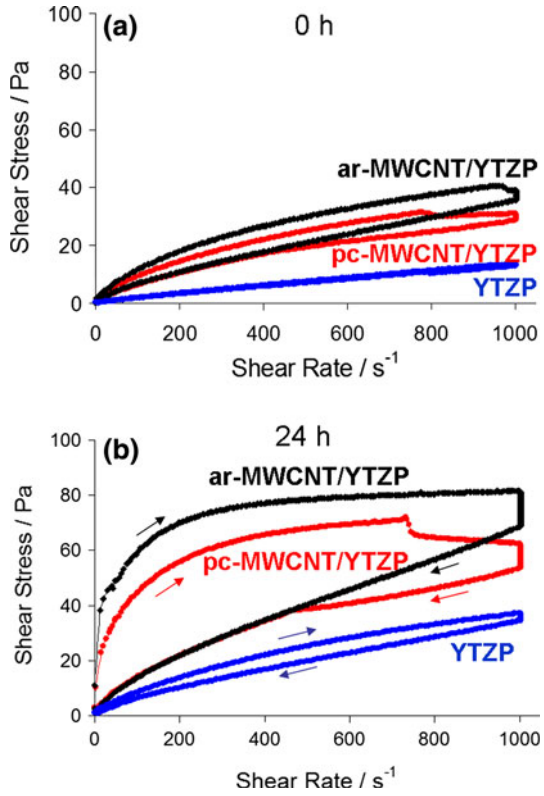

Fig. 4 Flow curves of the 65 wt% fresh and aged suspensions prepared with YTZP and MWCNT (ar-MWCNT or pc-MWCNT)

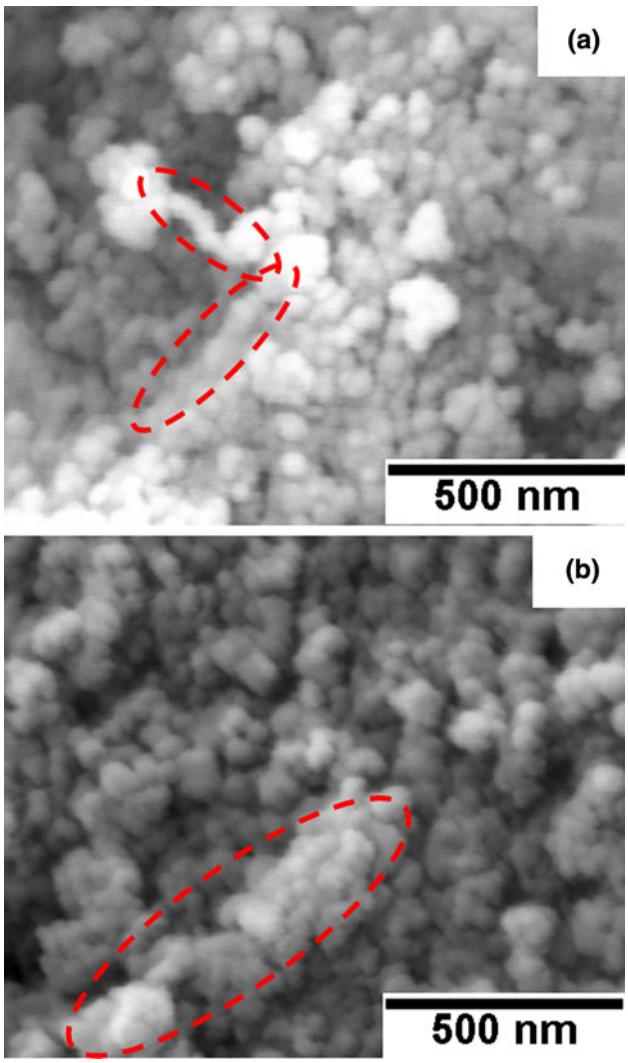

Fig. 5 FEG-SEM micrographs of the green fracture surface of ar-MWCNT/YTZP (**a**) and pc-MWCNT/YTZP (**b**)

higher sintered density (98% TD) as compared to that of the YTZP/ar-MWCNT samples (95.7% TD) (see Table 2).

Figure 7 shows the SEM microstructure of the fracture surfaces of the YTZP/ar-MWCNT and YTZP/pc-MWCNT. Even though the relative densities of the samples are very high, grain pull-out creates porous fracture surfaces, as shown on the SEM images. The YTZP/pc-MWCNT samples show a finer microstructure with an average grain size of 200 nm. The nanosized YTZP coating of the pc-MWCNT facilitates the dispersion and reduces the risk of agglomeration related to the hydrophobicity of the CNT.

The values of the Vickers' hardness and fracture toughness threshold are also presented in Table 2. YTZP/pc-MWCNT nanocomposites show approximately 10% higher hardness and K_{I0} values as compared to the YTZP/ar-MWCNT ones. When these data are compared to the corresponding values of YTZP samples [17] (12.5 ± 0.1 GPa and 3.8 ± 0.1 MPam$^{1/2}$, for Vickers hardness and fracture threshold (K_{I0}), respectively), it can be seen that K_{I0} of the YTZP/pc-MWCNT nanocomposites increases more than 15% compared to the YTZP samples, although the hardness suffers a decrease of 4%. This loss in hardness with the addition of CNT is in agreement with the results of other authors [6–19]. SEM pictures of Fig. 8 show the morphology of the cracks generated by the Vickers' indentation. As reported by other authors for carbon CNT/alumina composites, the increase in toughness of the YTZP/ar-MWCNT and YTZP/pc-MWCNT nanocomposites can be attributed to the bridging of cracks when they approach the CNT [24, 34]. The crack-bridging effect is more noticeable for the YTZP/pc-MWCNT samples, as pointed out on Fig 8b. This is thought to be due to the existence of a bond between the CNT and the zirconia matrix that ensures a good load transfer.

4 Conclusions

Commercial ar-MWCNT were partially coated with nanosized YTZP by a hydrothermal route, improving the wettability and dispersibility in aqueous medium, and thus the slip casting performance. Colloidal processing has been demonstrated to be suitable for the preparation of

Table 2 Properties of ar-MWCNT/YTZP and pc-MWCNT/YTZP composites

	Density (%TD)		Vickers hardness (GPa)	Fracture threshold (K_{I0}) ($MPam^{1/2}$)
	Green	Sintered		
ar-MWCNT/YTZP	42.9 ± 0.2	95.7 ± 0.1	11.0 ± 0.1	4.0 ± 0.1
pc-MWCNT/YTZP	42.7 ± 0.2	98.0 ± 0.1	12.0 ± 0.1	4.4 ± 0.1

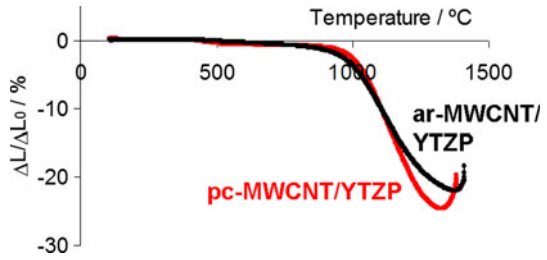

Fig. 6 Dynamic sintering studies of ar-MWCNT/YTZP and pc-MWCNT/YTZP samples

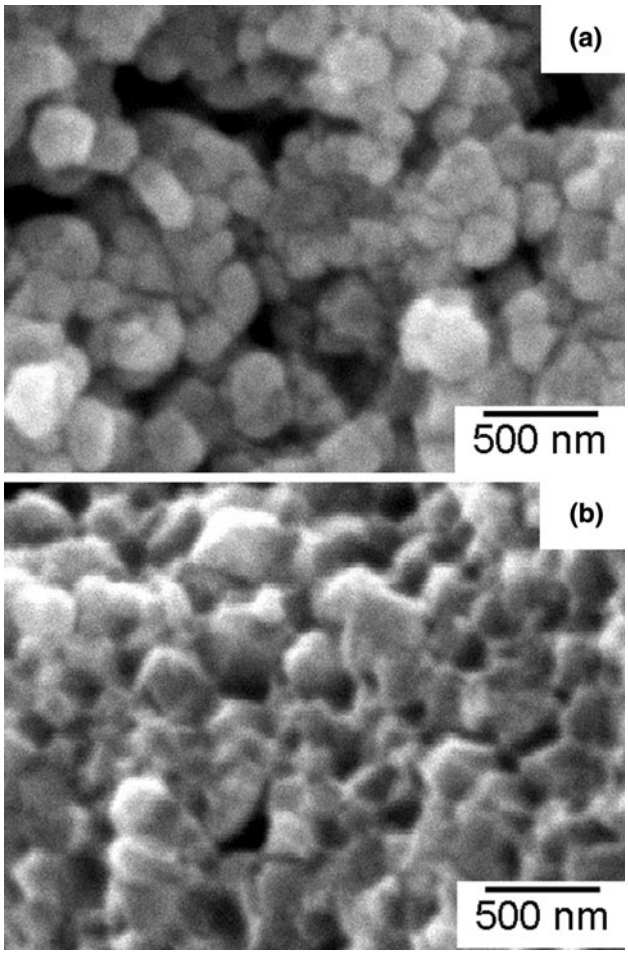

Fig. 7 SEM micrographs of the sintered microstructure of: 1 vol.% ar-MWCNT/YTZP (**a**) and 1 vol.% pc-MWCNT/YTZP (**b**) composites

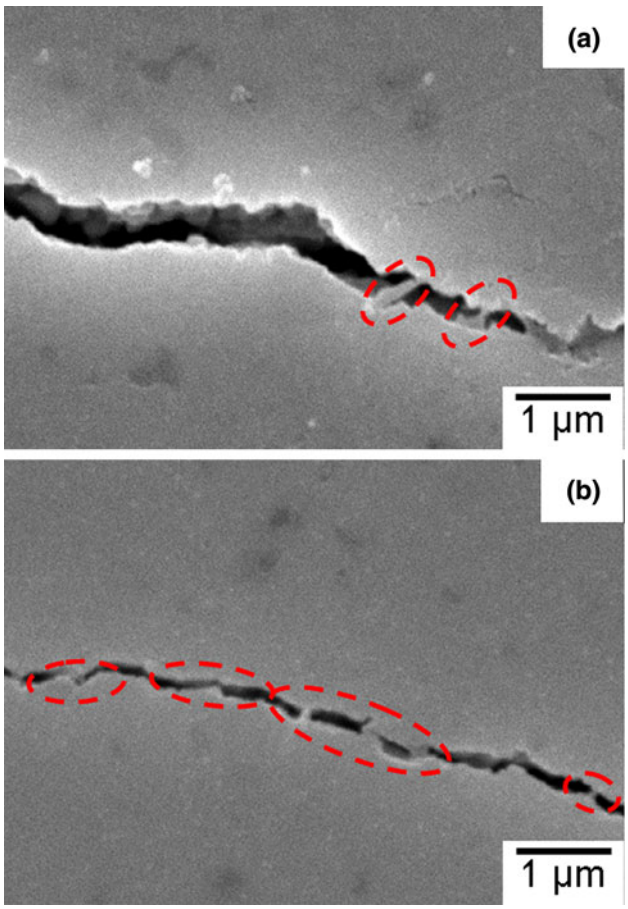

Fig. 8 SEM micrographs of the cracks generated by the Vickers indentation for: ar-MWCNT/YTZP (**a**) and pc-MWCNT/YTZP (**b**)

nanocomposites with a homogeneous dispersion of CNT in the ceramic matrix.

Dense bodies with 98% TD and final average grain size of ~200 nm were obtained for YTZP/pc-MWCNT nanocomposites after sintering at 1350°C in Ar atmosphere, while the YTZP/ar-MWCNT samples had lower densities (95.7% TD).

Although further work has to be carried out, the YTZP/pc-MWCNT materials present a higher increase in toughness and hardness than the YTZP/ar-MWCNT materials. This is possibly due to the increase in the wettability of the pc-MWCNT in the YTZP matrix and to the good load transfer between the pc-MWCNT and YTZP matrix that produces a stronger crack-bridging effect.

The results open a new path for the dispersion of higher pc-MWCNT contents in the YTZP matrix, that will be studied in future work. These new materials should offer better properties for the biomedical applications of the YTZP and, hence, longer lifetime and higher reliability.

Acknowledgments Supported by Spanish Ministry of Science and Innovation (project CIT-420000-2008-7 and Ramón y Cajal fellowship, RYC-2008-03523), Basque Government (PI-2004-2, BF105.R2.555 and Etortek: Nanomaterials).

References

1. Deville S, Gremillard L, Chevalier J, Fantozzi G. A critical comparison of methods for the determination of the aging sensitivity in biomedical grade yttria-stabilized zirconia. J Biomed Mater Res B Appl Biomater. 2005;72:239–45.
2. Matsui K, Horikoshi H, Ohmichi N, Ohgai M. Cubic-formation and grain-growth mechanism in tetragonal zirconia polycrystal. J Am Ceram Soc. 2003;86:1401–8.
3. Chevalier J. What future for zirconia as a biomaterial? Biomaterials. 2006;27:535–43.
4. Curtin WA, Sheldon BW. CNT-reinforced ceramics and metals. Mater Today. 2004;7:44–9.
5. Mayo M. Processing of nanocrystalline ceramics from ultrafine powders. Int Mater Rev. 1996;41:85–115.
6. Streicher RM, Schmidt M, Fiorito S. Nanosurfaces and nanostructures for artificial orthopedic implants. Nanomedicine. 2007; 2:861–74.
7. Iijima S. Helical microtubules of graphitic carbon. Nature. 1991; 354:56–8.
8. Zhan GD, Mukherjee AK. Carbon nanotube reinforced alumina-based ceramics with novel mechanical, electrical, and thermal Properties. Int J Appl Ceram Technol. 2004;1:161–9.
9. Zhan GD, Mukherjee AK. Processing and characterization of nanoceramic composites with interesting structural and functional properties. Rev Adv Mater Sci. 2005;10:185–96.
10. Wei T, Fan Z, Luo G, Wei F. A new structure for multi-walled carbon nanotubes reinforced alumina nanocomposite with high strength and toughness. Mater Lett. 2008;62:641–4.
11. Cha SI, Kim KT, Le KH, Mo CB, Hong SH. Strengthening and toughening of carbon nanotube reinforced alumina nanocomposite fabricated by molecular level mixing process. Scripta Mater. 2005;53:793–7.
12. Zhan GD, Kuntz JD, Wan J, Mukherjee K. Single-wall carbon nanotubes as attractive toughening agents in alumina-based nanocomposites. Nature Mater. 2003;2:38–42.
13. Balani K, Zhang T, Karakoti A, Li WZ, Seal S, Agarwal A. In situ carbon nanotube reinforcements in plasma sprayed aluminum oxide nanocomposite coating. Acta Mater. 2008;56:571–9.
14. Fan J, Zhao D, Wu M, Xu Z, Song J. Preparation and microstructure of multi-wall carbon nanotubes toughened Al_2O_3 composite. J Am Ceram Soc. 2006;89:750–3.
15. Sun J, Gao L, Iwasa M, Nakayama T, Niihara K. Failure investigation of carbon nanotube/3Y-TZP nanocomposites. Ceram Int. 2005;31:1131–4.
16. Duszová A, Dusza J, Tomásek K, Blugan G, Kuebler J. Microstructure and properties of carbon nanotube/zirconia composite. J Eur Ceram Soc. 2008;28:1023–7.
17. Garmendia N, Santacruz I, Moreno R, Obieta I. Slip casting of nanozirconia/MWCNT composites using a heterocoagulation process. J Eur Ceram Soc. 2009;29:1939–45.
18. Sun J, Gao L. Development of a dispersion process for carbon nanotubes in ceramic matrix by heterocoagulation. Carbon. 2003; 41:1063–8.
19. Geuzens E, Vanhoyland G, Haenb JD, Mullens S, Luyten J, Van Bael MK, et al. Synthesis of zirconia-alumina and alumina-zirconia core-shell particles via a heterocoagulation mechanism. J Eur Ceram Soc. 2006;26:3133–8.
20. Garmendia N, Bilbao L, Múñoz R, Imbuluzqueta G, García A, Bustero I, et al. Zirconia coating of carbon nanotubes by a hydrothermal method. J Nanosci Nanotechnol. 2008;8:5678–83.
21. Garmendia N, Arteche A, García A, Bustero I, Obieta I. XRD study of the effect of the processing variables on the synthesis of nanozirconia in the presence of MWCNT. J Compos Mater. 2009;43:247–56.
22. Garmendia N, Bilbao L, Muñoz R, Goikoetxea L, García A, Bustero I, et al. Nanozirconia partially coated MWNT: nanostructural characterization and cytotoxicity and lixiviation study. Key Eng Mater. 2008;361:775–8.
23. Sanchez-Paisal Y, Sanchez-Portal D, Garmendia N, Muñoz R, Obieta I, Arbiol J, et al. Zr-metal adhesion on graphenic nanostructures. Appl Phys Lett. 2008;93:053101.
24. Jiang D, Thomson K, Kuntz JD, Ager JW, Mukherjee AK. Effect of sintering temperature on a single-wall carbon nanotube-toughened alumina based nanocomposite. Scripta Mater. 2007;56: 959–62.
25. Padture NP, Curtin WA. Comment on "Effect of sintering temperature on a single-wall carbon nanotube-toughened alumina based nanocomposite". Scripta Mater. 2008;58:989–90.
26. Jiang D, Mukherjee AK. Response to comment on "Effect of sintering temperature on a single-wall carbon nanotube-toughened alumina based nanocomposite". Scripta Mater. 2008;58: 991–3.
27. Duszová A, Dusza J, Tomásek K, Morgiel J, Blugan GS, Kübler J. Zirconia/carbon nanofiber composite. Scripta Mater. 2008;58: 520–3.
28. Gatto A. Critical evaluation of indentation fracture toughness measurements with Vickers indenter on ceramic matrix composite tools. J Mat Proc Tech. 2006;174:67–73.
29. Liang KM, Torrecillas R, Orange G, Fantozzi G. Determination of $K_{(ISCC)}$ by indentation in ceramics. J Mat Sci. 1990;25: 5077–80.
30. Benzaid R, Chevalier J, Saâdoui M, Fantozzi G, Nawa M, Diaz LA, et al. Fracture toughness and slow crack growth in a ceria stabilized zirconia-alumina nanocomposite for medical applications. Biomaterials. 2008;5:3636–41.
31. Chevalier J, De Aza AH, Fantozzi G, Schehl M, Torrecillas R. Extending the lifetime of orthopaedic implants. Adv Mater. 2000;12:1619–21.
32. Anstis GR, Chantikul P, Lawn BR, Marshal DB. A critical evaluation of indentation techniques for measuring fracture toughness: I, direct crack measurements. J Am Ceram Soc. 1981;64: 533–8.
33. Fengqiu T, Xiaoxian H, Yufeng Z, Jingkun G. Effect of dispersants on surface chemical properties of nanozirconia suspensions. Ceram Int. 2000;26:93–7.
34. Yamamoto G, Omori M, Hashida T, Kimura H. A novel structure for carbon nanotube reinforced alumina composites with improved mechanical properties. Nanotechnol. 2008;19:315708–14.